EPJ Web of Conferences **45**, 01043 (2013)
DOI: 10.1051/epjconf/20134501043

Visualization and modal decomposition of vortex street behind circular cylinder

T. Hyhlík[1,a] , P. Železný[1] and, J. Čížek[1]

[1]CTU in Prague, FME, Department of Fluid Dynamics and Thermodynamics, Technická 4, 166 07, Prague

Abstract. Time resolved particle image velocimetry measurement of vortex street behind circular cylinder was carried out. Vortex street was measured for Reynolds numbers up to few thousands. Obtained results were processed by visualizations of moving particles and by standard evaluation of vector fields from the set of images. Modal decomposition of measured flow field was done using propper orthogonal decomposition where the structure of energetically most important modes was identified for several Reynolds numbers. The values of Strouhal number was analyzed from temporal evolution of dominant modes obtained using proper orthogonal decomposition.

1 Introduction

It is well known that wake flow behind circular cylinder has direct engineering significance. The vortex shedding in the wake leads to large fluctuations in the pressure field which can cause structural vibrations and acoustic noise. Although investigation of vortex streets behind circular cylinder is already traditional subject of research in fluid dynamics [1], recent analyses [2] and progress in measurement techniques and in numerical modelling linked with the development of new theoretical models leads to extension of knowledge in this field.

The analysis of the dynamics of complex flow is still challenge due to its unsteady three-dimensional nature. It is important to characterise and quantify the properties of the flow, so that desired and undesired effects can be identified, understood and possibly controlled.

Circular cylinder wake is very complex. It involves the interactions of three shear layers, namely a boundary layer, a separating free shear layer and a wake [2]. Hydrodynamic instabilities which develop in the near wake are of at least two types, Kelvin–Helmholtz like instability in the separated shear layer and von Kármán instability in the wake. The review [2] summarizes results considering circular cylinder.

2 Experimental setup

Experiments were conducted in low speed closed-circuit wind tunnel with test section of 0.2 × 0.3 m with maximum velocity of 42 ms^{-1}.

[a] tomas.hyhlik@fs.cvut.cz

Circular cylinder is placed in the test section between two panels made from transparent plexiglass. Transparent plexiglass was chosen because of the use of visualization techniques for the measurement of the flow field behind the cylinder.

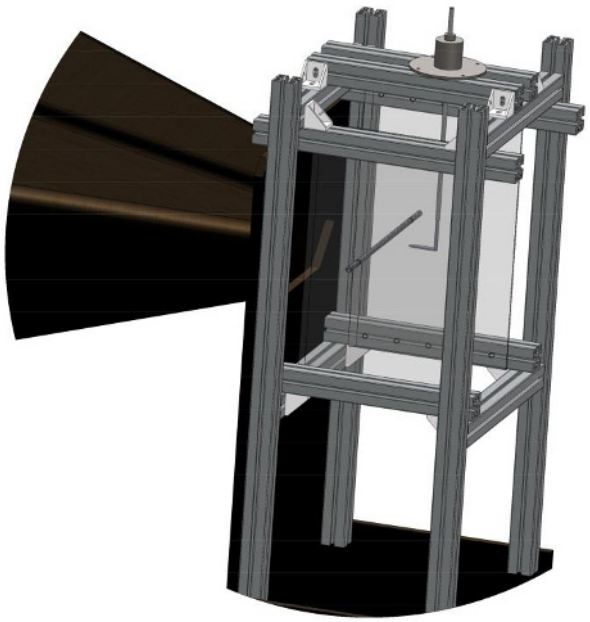

Fig. 1. Test section with cylinder and measuring probe

There is an arrangement of test section with circular cylinder and measuring probe in the figure 1.

Measurement was done by using time resolved particle image velocimetry (TR-PIV). 2D TR-PIV was used for our measurement. TR-PIV consists of fast camera (CMOS, 1280 × 1024, maximum frequency at maximum resolution is 1040 fps, internal memory of 4GB), an optical amplifier (Hamamatsu C9548) and continuous light sources (high performance laser diode).

Nikon macro lense (AF Micro-Nikkor 60mm f/2.8D) with conversion lense was used to capture the frames.

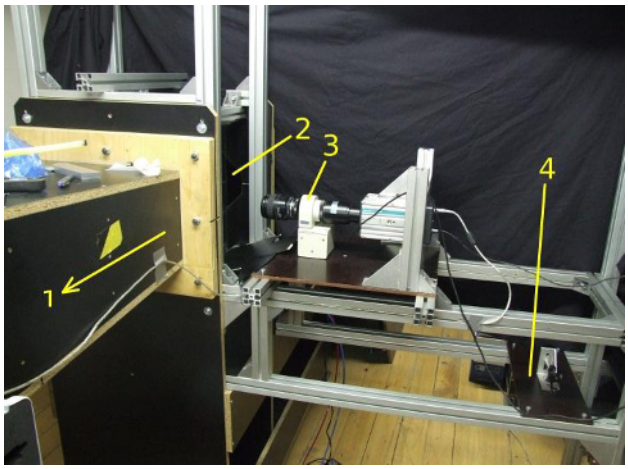

Fig. 2. Experimental setup: 1 – flow direction, 2 – test section, 3 - optical amplifier and optics, 4 - half cylinder lens

The figure 2 shows an arrangement of PIV system close to the test section with a camera, optical amplifier, lens, half cylinder lens and other necessary components. Seeding particles were delivered to the wind tunnel in the form oil mist from the device Safex in front of the axial fan. The view of light sheet with visualized seeding particles is in the figure 3. The wake behind circular cylinder visualized using light sheet is partly visible in the above mentioned figure which was taken by an ordinary camera.

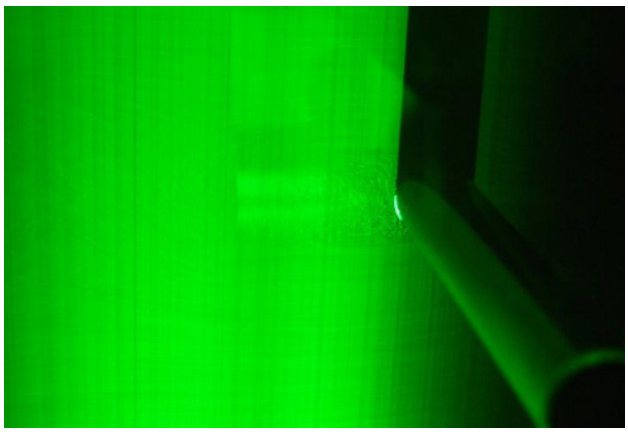

Fig. 3. Light sheet view; flow is from the right to the left

3 Visualizations

The first goal was to visualize flow field in the cylinder wake. Due to the size of the evaluated area starts diameter of circular cylinder at 10 mm. The cylinder is placed on the left just before the snapshot. The frame rate was typically chosen between 1200 and 1400 Hz. There are visualized flow field in the figures 4, 5 and 6. Visualizations are created by summing and inverting several successive frames. Basic characteristics connected with flow around cylinder like wake length and volume, separation points, vortex size and position can be read from these pictures.

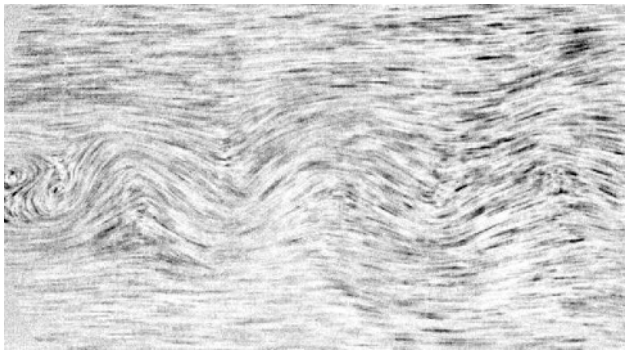

Fig. 4. *Re = 429, d = 10 mm*

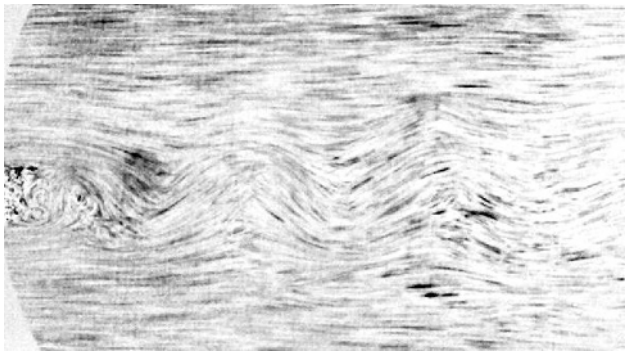

Fig. 5. *Re = 824, d = 10 mm*

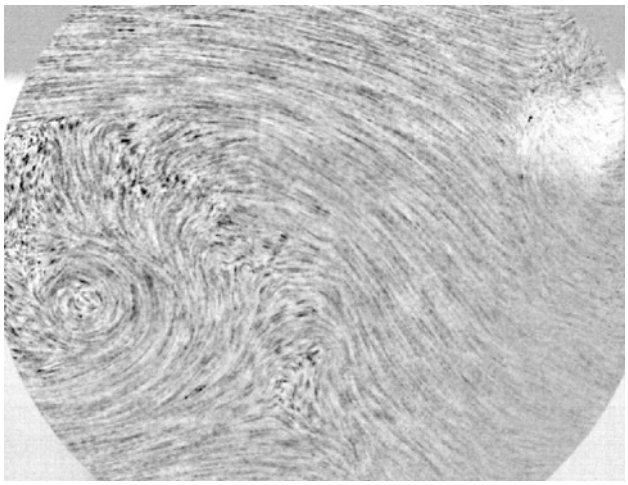

Fig. 6. *Re = 3667, d = 50 mm*

A closer look at a longer sequence of images allowed to see three-dimensional character of the flow field at considered Reynolds numbers. This effect can be manifested by periodic disappearance and reappearance of some particles in certain places.

4 Modal decomposition

Modal decomposition can be used to analyse the data and subsequently can be used for the development of low-dimensional models which capture the essential flow physics.

Let's start with set of N flow fields from experiment which are equidistantly sampled [3] with timestep Δt

$$\boldsymbol{U} = [\, \boldsymbol{u}_1 \ \ldots \ \boldsymbol{u}_{N-1}\, \boldsymbol{u}_N \,]. \qquad (1)$$

A common modal decomposition technique for identifying coherent structures is the proper orthogonal decomposition (POD) method [3-5]. The main objective in POD is to obtain an optimal low-dimensional basis for representing an ensemble of high-dimensional experimental or simulation data. This method is capable of extracting information from snapshots of the flow field and is thus applicable to experimental and numerical data. POD decomposes a given flow field into an orthonormal system of spatial modes $\boldsymbol{X}$ and corresponding mode amplitudes $\boldsymbol{T}$

$$\boldsymbol{U} = \boldsymbol{X}\,\boldsymbol{T}. \qquad (2)$$

The method determines the most energetic structures by diagonalizing the correlation matrix computed from the snapshots

$$\boldsymbol{C} = \boldsymbol{U}^{\mathrm{T}}\,\boldsymbol{W}\,\boldsymbol{U}, \qquad (3)$$

where $\boldsymbol{W}$ is weighting matrix with cell volumes on diagonal. The evaluation of POD modes leads to the solution of eigenvalue problem [3]

$$\boldsymbol{C}\,\boldsymbol{v}_{\mathbf{i}} = \lambda_{\mathrm{i}}\,\boldsymbol{v}_{\mathbf{i}}, \qquad i = 1, \ldots, N. \qquad (4)$$

Eigenvalues λ_{i} are then proportional to the energy of given mode. Temporal amplitude $\boldsymbol{T}$ of the mode can be obtained by rescaling of orthonormal eigenvector $\boldsymbol{v}_{\mathbf{i}}$ and spatial modes $\boldsymbol{X}$ are evaluated using inversion [3] from equation (2).

5 POD modes

POD modes has been evaluated from the data sets obtained using standard adaptive cross-correlation where interrogation area was set to 32 × 32 pixel and overlap of 75% in both directions was chosen.

The figure 7 shows normalized energy of first twenty POD modes for the case of *Re = 429*. It is visible that the most of energy (93.56%) is included in the first mode, second mode includes 1.13% and the third mode includes 1.08%. Every other mode includes significantly less energy then the first three.

There is a velocity field of the first mode in the figure 8. The velocity field of the first mode is in fact averaged flow field. The errors close to the upper left and lower left corners are caused by inaccuracy of the PIV method close to the boundary of evaluated area.

The distribution of x component of velocity for the both second mode and third mode is presented in the figure 9 and in the figure 10. The structure of both spatial modes is very similar. From these pictures is visible that the topological structure is only slightly shifted in the direction of x axis.

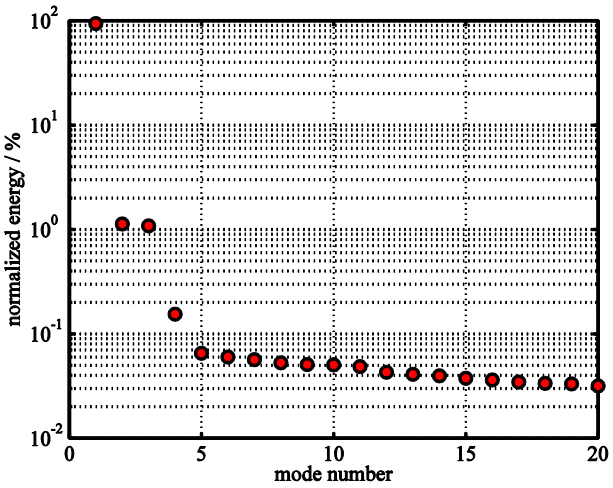

Fig. 7. Energy of POD modes, *Re = 429*

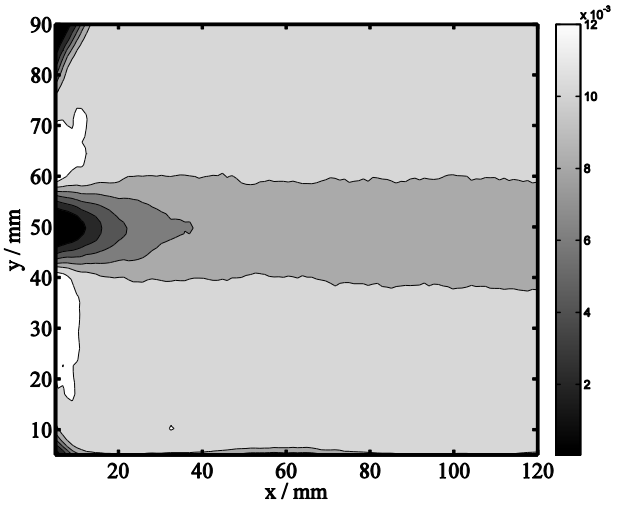

Fig. 8. Mode 1, velocity magnitude, *Re = 429*

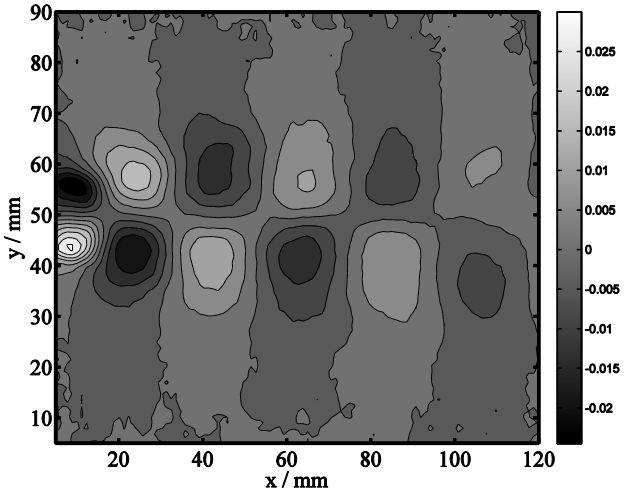

Fig. 9. Mode 2, x-velocity component, *Re = 429*

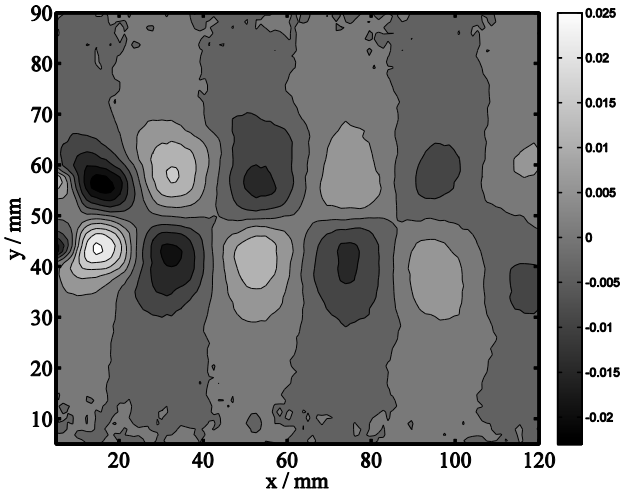

Fig. 10. Mode 3, x-velocity component, *Re = 429*

The distribution of temporal amplitudes of the second and third mode is shown in the figure 11. The picture shows phase shift of temporal amplitude of third mode against second mode. Strouhal number was evaluated for both modes using FFT. The value of Strouhal number is *St = 0.2236* for both modes. The inaccuracy of Strouhal number is caused by the imperfection in the measurement of reference velocity

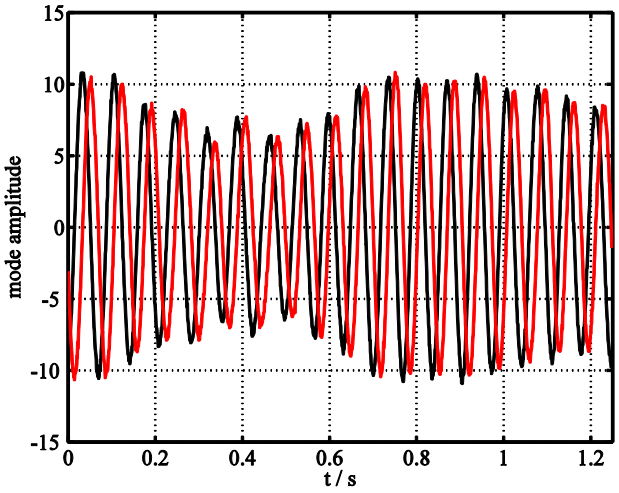

Fig. 11. Temporal amplitudes of mode 2 and 3, *Re = 429*

There are vector lines of the second and third modes in the figure 12. Figure shows x direction shift of the vector lines of third mode against vector lines of second mode.

Figures 9, 10, 11 and 12 depict cooperation of second and third POD mode which represent von Kármán type of instability in the circular cylinder wake.

The measurement was done up to Reynolds number (Re = 3667). Behaviour is very similar to the low Reynolds number case. There are errors close to the right boundary and close to the upper left corner as was previously mentioned.

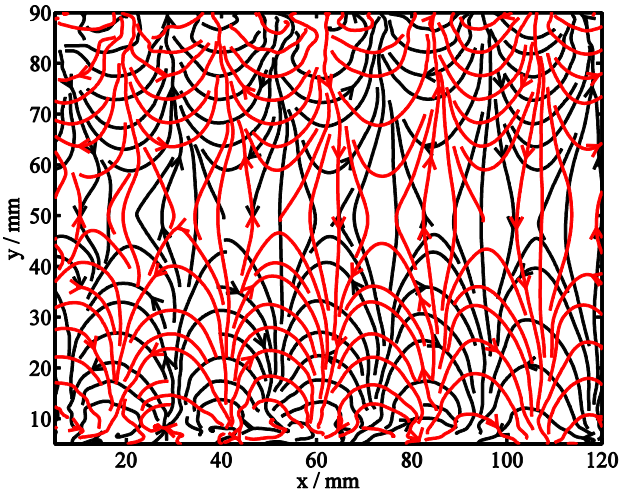

Fig. 12. Vector lines of mode 2 and 3, *Re = 429*

6 Conclusion

Investigation of the flow field behind circular cylinder and the analysis of the structure of the cylinder wake from the point of view of proper orthogonal decomposition has been made. The visualization of flow field based on direct processing of obtained snapshots was also presented. The focus was placed mainly on the modal decomposition of the measured data obtained using TR-PIV method. It has been shown that von Kármán type of instability is strongly connected with second and third POD mode. The frequency of vortex shedding corresponds with frequency obtained from the FFT analysis of the vectors of temporal amplitudes of second and third POD mode. Von Kármán type of instability was identified using POD for Reynolds numbers from few hundreds to more than three and half thousand.

7 Acknowledgement

The support from the Grant Agency Academy of Sciences of the Czech Republic under grant No. IAA200760801 is gratefully acknowledged.

References.

1. V. Strouhal, Ann. Phys. Chem. **10**,(1878)
2. C. H. K. Williamson, Annu. Rev. Fluid. Mech, **28**, 477-539, (1996)
3. O. Frederich, D. M. Luchtenburg, *Seventh International Symposium On Turbulence and Shear Flow Phenomena*, (Ottawa, 2011)
4. J. L. Lumley, *Stochastic Tools in Turbulence*, (Academic Press, 1970)
5. L. Sirovich, Quaterly of Applied Mathematics, **XLV**, 3, (1987)